Nano Today (2009) 4, 359—373

available at www.sciencedirect.com

ScienceDirect

journal homepage: www.elsevier.com/locate/nanotoday

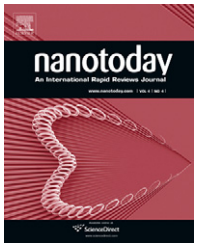

REVIEW

Synthesis and biomedical applications of hollow nanostructures

Kwangjin An, Taeghwan Hyeon*

National Creative Research Initiative Center for Oxide Nanocrystalline Materials and School of Chemical and Biological Engineering, Seoul National University, Seoul 151-744, Republic of Korea

Received 18 May 2009; received in revised form 25 June 2009; accepted 30 June 2009

KEYWORDS
Hollow;
Nanoparticle;
Kirkendall effect;
Galvanic replacement;
Etching;
Biomedical applications;
Template synthesis;
Drug delivery vehicle

Summary Hollow nanostructures have attracted tremendous attention from researchers in various disciplines because their high surface to volume ratio and large pore volume are highly desirable for many technological applications including drug delivery system. Several colloidal synthetic methods have been used to synthesize various hollow nanostructures. These synthetic approaches are mainly categorized into four main classes according to how the hollow structure is formed: the Kirkendall effect, chemical etching, galvanic replacement, and template-mediated approach. The large pores inside the hollow nanostructures can encapsulate and release various drugs and biomolecules, while the surface of the nanostructure can be functionalized for drug targeting or bio-labeling. These features make the hollow nanostructures a unique and promising candidate as multifunctional drug delivery vehicles. This review article covers recent progress concerning the synthesis of hollow nanostructures with their sizes smaller than 200 nm and their biomedical applications including specific targeting, imaging, and controlled release of therapeutics for simultaneous diagnosis and therapy.

For the last decade, hollow nanostructures with a controlled pore volume and shell thickness have emerged as an important class of nanomaterials [1—4]. These hollow nanostructures have much higher surface to volume ratio compared to the solid counterparts with the same sizes, which would be beneficial for applications including catalysis, energy storage and conversion, and biomedicine [1].

The most popular method to synthesize the hollow nanostructures is template-mediated approaches [5]. By coating the surface of the template particles with desired materials and removing the template by a post-treatment, various hollow particles can be easily obtained. Silica particles and polymer beads are widely used hard template materials. There are various methods to coat materials on these hard templates: layer-by-layer assembly [6,7], chemical deposition [8,9], adsorption [10—12], casting [13], and atomic layer deposition [14]. Various soft templates have been also employed for the synthesis of hollow nanostructures, including microemulsions formed in a two-phase solution [15,16], gas bubbles in liquid [17,18], and micelles (or vesicles) assembled by surfactants or supramolecules [19,20]. Recently, Lou and co-workers comprehensively reviewed the synthesis and applications of hollow micro- and nanos-

* Corresponding author. Tel.: +82 2 880 7150; fax: +82 2 886 8457.
E-mail addresses: akj007@snu.ac.kr (K. An), thyeon@snu.ac.kr (T. Hyeon).

1748-0132/$ — see front matter © 2009 Elsevier Ltd. All rights reserved.
doi:10.1016/j.nantod.2009.06.013

Table 1 Synthetic strategies for the hollow nanomaterials.

Applied methods	Hollow materials	Initial materials (templates)	Shape	Ref.
Nanoscale-Kirkendall effect	Co_3S_4, Co_9S_8, CoSe	Co	Sphere	[21,33]
	Pt—CoO	Pt—Co	Yolk—shell	[21]
	Fe_3O_4	Fe—Fe_3O_4	Sphere	[34]
	γ-Fe_2O_3	Fe	Sphere	[35,44]
	$ZnAl_2O_4$	ZnO—Al_2O_3	Tube	[36,37]
	$CoSe_2$, Co_3S_4, CoTe	Co	Necklace	[38]
	Ni_2P, Co_2P	Ni, Co	Sphere	[39,40]
	CeO_2—ZrO_2	CeO_2—ZrO_2	Sphere, box	[41]
	FePt—CoS_2	FePt—Co	Yolk—shell	[98]
	FePt—Fe_2O_3	FePt—Fe_2O_3	Yolk—shell	[99]
	Au—Fe_2O_3	Au—Fe_2O_3	Yolk—shell	[42]
	Pt—Cu	Pt—Cu	Core—shell	[45]
	$Cu_{2-x}Se$	Cu_2O	Sphere	[46]
	CuO	Cu	Tube	[47]
	Ag—Ag_2Se, Ag_2Se	Ag	Sphere, tube	[48,49]
	PbS, Pb—PbS, Pb—Ag	Pb	Sphere	[50]
	CdS	Cd	Sphere	[43]
	Co_3S_4	$Co(CO_3)_{0.35}Cl_{0.20}(OH)_{1.10}$	Tube	[51]
	ZnS	ZnO	Sphere	[52]
	ZnO	Zn	Sphere	[53]
Chemical etching	Fe	Fe	Box, frame	[54]
	Fe-phosphide	Fe_3O_4, α-Fe_2O_3	Sphere, box	[22]
	Mn-phosphide	MnO	Sphere, multi-pods	[22]
	Mn—Fe-phosphide	$MnFe_2O_4$	Sphere	[22]
	ZnO, Au—ZnO, Pt—ZnO, Au—Pt—ZnO	ZnO	Sphere	[57]
	Co	Co	Box, frame	[55]
	Pd	Pd	Box, frame	[56]
	Cu_2O	Cu_2O	Dodecahedral, frame	[58]
Galvanic replacement	Au	Ag	Box, cage, triangular ring, prism-shaped box, tubes, multiple-walled shell or tube	[3,4,62—68]
	Pd—Ag, Pt—Ag	Ag	Box, frame	[69]
	Au, Ag, Pt, AuPt, CoPt	Co	Sphere	[70—75]
	AuPt,	Co	Necklace	[71]
	Au, Pt, Pd	Co	Necklace	[76]
Nanotemplate	α-Fe_2O_3, Fe_3O_4	β-FeOOH	Capsule	[23]
	α-Fe_2O_3	Silica	Sphere	[77]
	Silica	Fe_3O_4	Sphere	[78]
	α-FeOOH	Organics	Tube	[80]
	Co	CoO	Parallelepiped	[81]

tructures [1]. Usually, the hollow structures obtained via a template-mediated approach using silica or polymer particles as the templates are often larger than 200 nm because it is hard to make smaller sized template particles. In addition to this size limitation, the template-mediated method has other disadvantages; the post-treatment necessary to remove the templates adds complexity to the whole synthetic process and increases the chance of the structural deformation as well as the introduction of impurities. In order to overcome these limitations, simple and novel strategies are highly desired. In this review, we will focus on the colloidal synthesis of high-quality hollow nanostructures with their sizes *smaller than* 200 nm. The structures of our interest encompass nanoframes and nanocages with porous walls as well as those with solid walls. The synthetic approaches are categorized into four main types according to how the hollow nanostructures are formed: the Kirkendall effect [2,21], chemical etching [22], galvanic replacement [3,4], and template-mediated approach (see Table 1). All of these approaches exploit nanoparticles as starting materials except for the nanotemplate-mediated approaches, where these starting nanomaterials play the role of the sacrificial templates that are dissolved or transformed to generate hollow nanostructures. Hollow nanostructures can find various biomedical applications including simultaneous diagnosis and therapy. The large pore volume inside the hollow nanostructures can be used to incorporate various drugs and biomolecules and release them in a controlled manner. At the same time, the surface of the hollow nanostructures can be readily functionalized with optical labels and targeting agents [3,4]. This review covers the recent progress on the synthesis and biomedical applications of various hollow nanostructures [23—30]. The first four sections describe the synthesis of hollow nanostructures using four different synthetic approaches followed by their various biomedical applications.

Nanoscale Kirkendall effect

In 1942, Kirkendall reported that net mass transport occurred across the interface between two different metal species upon annealing and vacancy-assisted hopping was proposed as the main mode of atomic transport [31]. At the interface, two metal species in contact have different diffusion rates resulting in the net flux of atoms from one side of the interface to the other. As atoms diffuse through the interface, vacancies move in the opposite direction and accumulate to form voids. The stress originated from an increase in the void volume during diffusion induces the porosity in the solid. This phenomenon is now known as the Kirkendall Effect. In 1947, Smigelkas and Kirkendall demonstrated that, at an elevated temperature, the difference between the diffusion rates of copper and zinc in brass led to the formation of pores in the species [32]. In 2004, Alivisatos and his co-workers reported exploiting the Kirkendall effect at the nanometer scale for the fabrication of hollow nanostructures [21]. In their report, cobalt nanocrystals were transformed to hollow chalcogenide nanocrystals by introducing either oxygen, sulfur, or selenium into the hot dispersion of cobalt nanocrystals. For example, the sulfidation of cobalt nanocrystals by the addition of elemental sulfur dissolved in organic solution resulted in the formation of hollow cobalt sulfide nanocrystals of either Co_3S_4 or Co_9S_8, depending on the molar ratio of sulfur and cobalt [21,33]. During the transformation, cobalt nanocrystals are first covered with a cobalt sulfide shell. Next, the diffusion of cobalt and sulfur atoms in opposite directions takes place at the surface of cobalt and cobalt sulfide. As the reaction proceeds, voids form in the cobalt side of the interface because the outward diffusion of cobalt atoms is faster than the inward diffusion of sulfur atoms. Similar intermediate

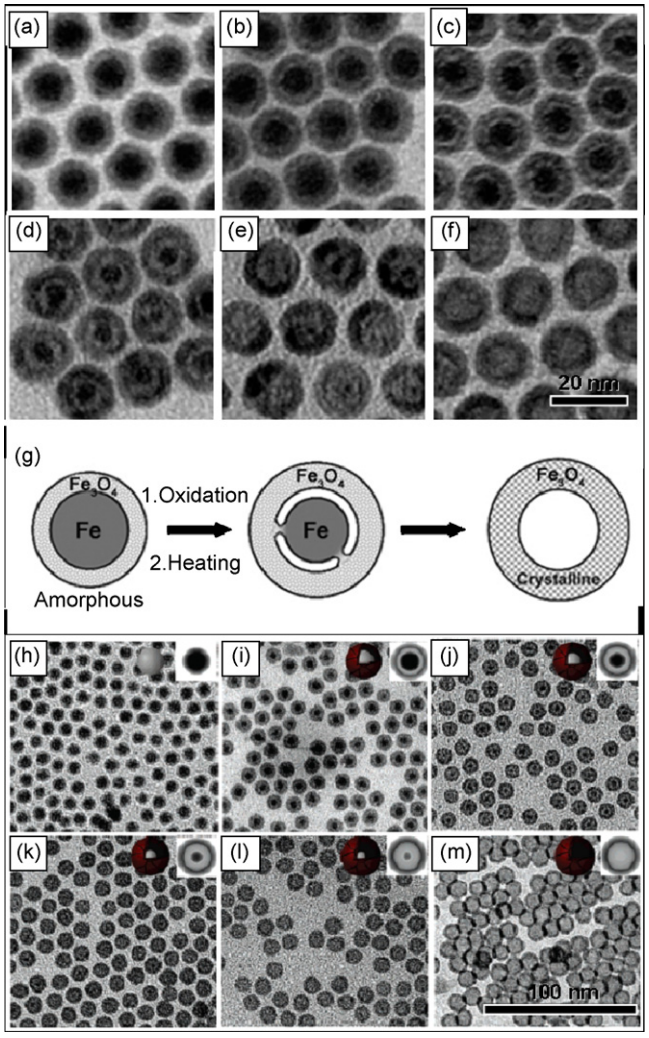

Figure 1 (a—f) TEM images showing the shape evolution of Fe—Fe_3O_4 core—shell nanoparticle (a) via Kirkendall effect. Core—shell—void intermediates obtained by the reaction for 1 h (b) and 2 h at 130 °C (c), and 40 min (d) and 80 min at 210 °C (e). Hollow Fe_3O_4 nanoparticles from the reaction for 120 min at 210 °C (f). (g) Schematic illustration showing the shape evolution from the core—shell to the hollow structure (reproduced with permission from [34], copyright 2007 Wiley-VCH). (h—m) TEM images showing the shape evolution of hollow iron/iron oxide nanoparticles exposed to dry 20% oxygen for 1 min at room temperature (h), 1 h (i) and 12 h at 80 °C (j), 5 min (k) and 1 h at 150 °C (l). Fully oxidized iron oxide nanocrystals were obtained by oxidation for 1 h at 350 °C (m) (reproduced with permission from [35], copyright 2007 American Chemical Society).

structures were observed in many other hollow nanomaterials. Peng and Sun observed a core–shell–void intermediate structure during the synthesis of hollow Fe_3O_4 nanocrystals [34]. In their report, they synthesized amorphous Fe–Fe_3O_4 nanoparticles (Fig. 1a) via thermal decomposition of $Fe(CO)_5$ in a hot organic solution and subsequent air oxidation. The controlled oxidation of Fe–Fe_3O_4 nanoparticles in the presence of an oxygen-transfer reagent, trimethylamine *N*-oxide, yielded monodisperse hollow Fe_3O_4 nanoparticles with controlled sizes via the nanoscale Kirkendall effect. It was observed that when the reaction was quenched by lowering the temperature in the middle of the reaction process, multiple voids were formed in the particle. By adjusting the reaction temperature and time, it was possible to obtain a series of intermediate structures from the solid particle to the core–shell–void, the yolk–shell, and, finally, the hollow structures, which is a good evidence for the Kirkendall effect. Fig. 1a–f show that the shape of the nanoparticles evolved from the core–shell to the hollow ones as the reaction time was increased, and as the temperature was raised, which is also illustrated in Fig. 1g. The Alivisatos group also synthesized a series of monodisperse iron–iron oxide core–void–shell and hollow iron oxide nanoparticles by the controlled oxidation under O_2 atmosphere adopting the nanoscale Kirkendall effect [35]. The reaction temperature and oxidation time allowed for precise tuning of the thickness of the oxide shell, as shown in Fig. 1h–m.

The Kirkendall effect can also be applied to fabricate 1-dimensional (1-D) hollow nanomaterials. Fan and their co-workers fabricated single crystalline $ZnAl_2O_4$ spinel nanotubes (Fig. 2a and b) with a diameter of ~40 nm and a wall thickness of ~10 nm using ZnO–Al_2O_3 core–shell nanowires as the starting material [36,37]. They proposed a model explaining the formation mechanism of their 1-D hollow structures, the so-called, ''Kirkendall effect + surface diffusion'' process [37]. According to the proposed model, the surface diffusion process is a dominant mass flow mode responsible for the enlargement of interior pores after their formation induced by the Kirkendall effect. Fig. 2c illustrates the different diffusion processes in the growth of hollow nanostructures. At the early stage, small Kirkendall voids are generated via bulk diffusion at the interface. When large numbers of voids contact the inner surface of the shell, the surface diffusion of the atoms of the core material becomes dominant along the skeletal bridges. Through the channels of the shell layer, the material exchange proceeds

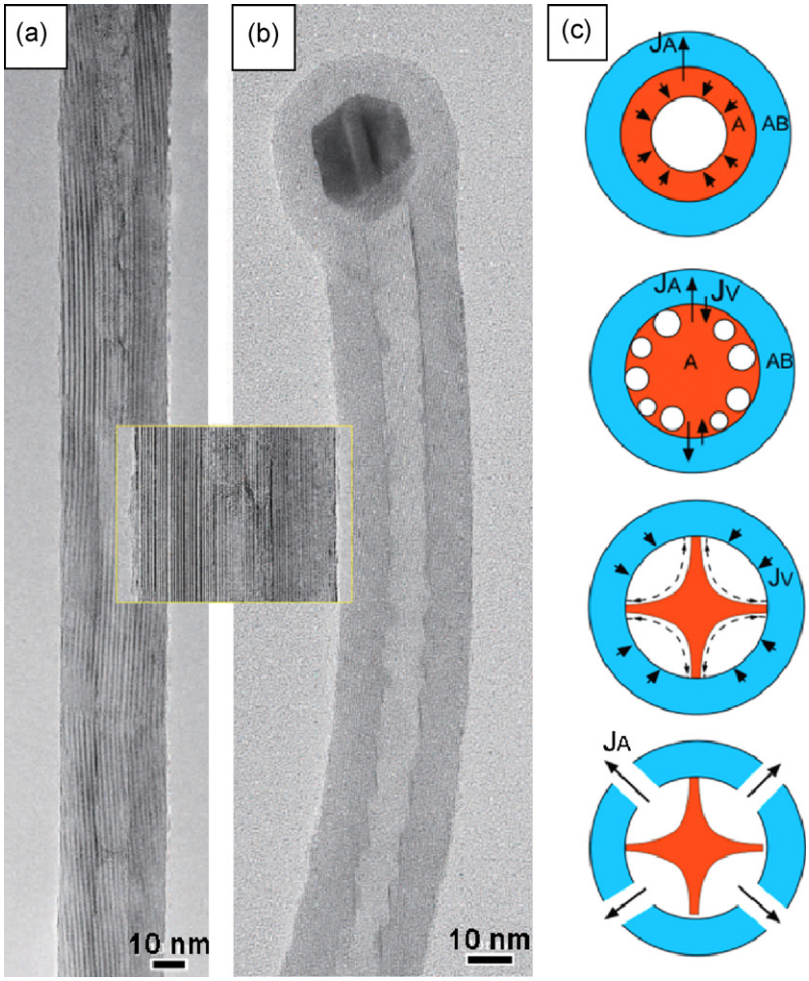

Figure 2 TEM images of (a and b) the $ZnAl_2O_4$ spinel nanotubes (reproduced with permission from [36], Copyright 2006 Nature Publishing Group) and (b) Schematic illustration showing the different diffusion processes in the growth of the hollow nanostructure (reproduced with permission from [2], copyright 2007 Wiley-VCH).

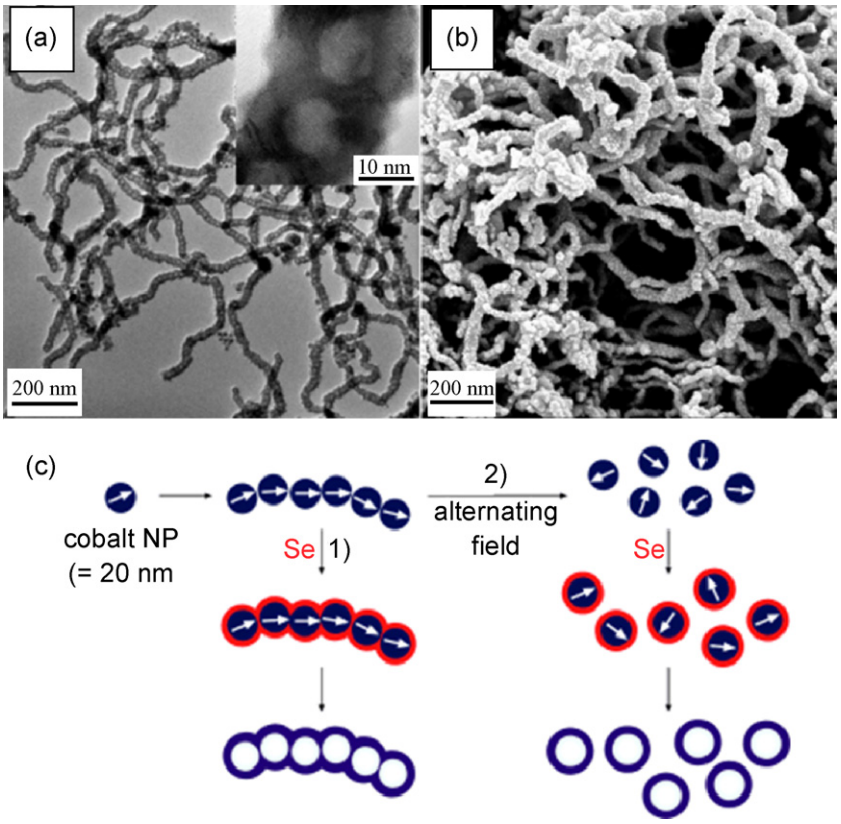

Figure 3 (a) TEM, HRTEM (inset), and (b) SEM image of the wires of hollow $CoSe_2$ nanocrystals. (c) Schematic illustration showing the formation of hollow $CoSe_2$ nanocrystals from cobalt nanoparticles in the (1) absence and (2) presence of an alternating magnetic field (reproduced with permission from [38], copyright 2006 Wiley-VCH).

via direct dissolution (in the solution phase) or evaporation (in the gas phase), generating the hollow nanostructure.

Xu et al. applied the nanoscale Kirkendall process to magnetically assembled 1-D hollow nanostructures of cobalt chalcogenides [38]. First, they assembled cobalt nanocrystals with the size of 20 nm into necklace-like structures by the magnetic dipolar interactions. Then, the cobalt nanocrystal assemblies were transformed to $CoSe_2$ hollow nanostructures retaining the chain-like shape via the Kirkendall process (Fig. 3). During the synthesis, by exerting an alternating magnetic field, a small number of individual hollow $CoSe_2$ nanocrystals were obtained, which were fractured from the chain, because the applied vibrational magnetic torque disrupted the dipolar interactions between the particles.

Several hollow nanostructures of oxides, sulfides, selenides, and phosphides have been synthesized by many researchers via the nanoscale Kirkendall effect [39—53]. For example, the Schaak and Chiang groups independently reported hollow Ni_2P nanoparticles synthesized from oleylamine-stabilized Ni nanoparticles in the presence of trioctylphosphine (TOP) [39,40]. The Li group fabricated CeO_2—ZrO_2 nanocages by reacting ceria nanospheres with zirconium (IV) in a glycol medium [41]. The Alivisatos group synthesized gold—iron oxide core—hollow—shell nanoparticles, in which the formation of the hollow oxide shell resulted from the oxidation of the iron shell by oxygen [42]. The same group also reported asymmetric Cd/CdS partial hollow structures, in which the unreacted Cd core and the coalesced vacancies were separated into two distinct spherical caps. It was attributed to the faster diffusion of cadmium atoms through the polycrystalline shells, compared to sulfur atoms [43]. They further extended the synthetic method of the hollow core—shell—void nanoparticles to generate various quasi-ternary superlattices [44]. Recently, Fan and co-workers reviewed the fabrication of nanotubes and hollow nanoparticles based on the Kirkendall effect and summarized various kinds of hollow nano- and micro-materials [2].

Chemical etching

Etching, or partial dissolution of the interior of nanoparticles, is another approach to synthesize hollow or porous nanomaterials. Several kinds of hollow nanomaterials synthesized via the selective etching process have been reported. The Hyeon group synthesized hollow iron nanoframes by thermal decomposition of a Fe(II)—stearate complex in the presence of sodium oleate and oleic acid at 380 °C (Fig. 4a) [54]. In this process, solid iron nanocubes are initially generated from the thermal decomposition of Fe(II)—stearate complex and subsequent reduction by the byproducts from the decomposition of oleic acid. These solid nanocubes were subsequently transformed into nanoframes with a hollow core. This transformation was attributed to

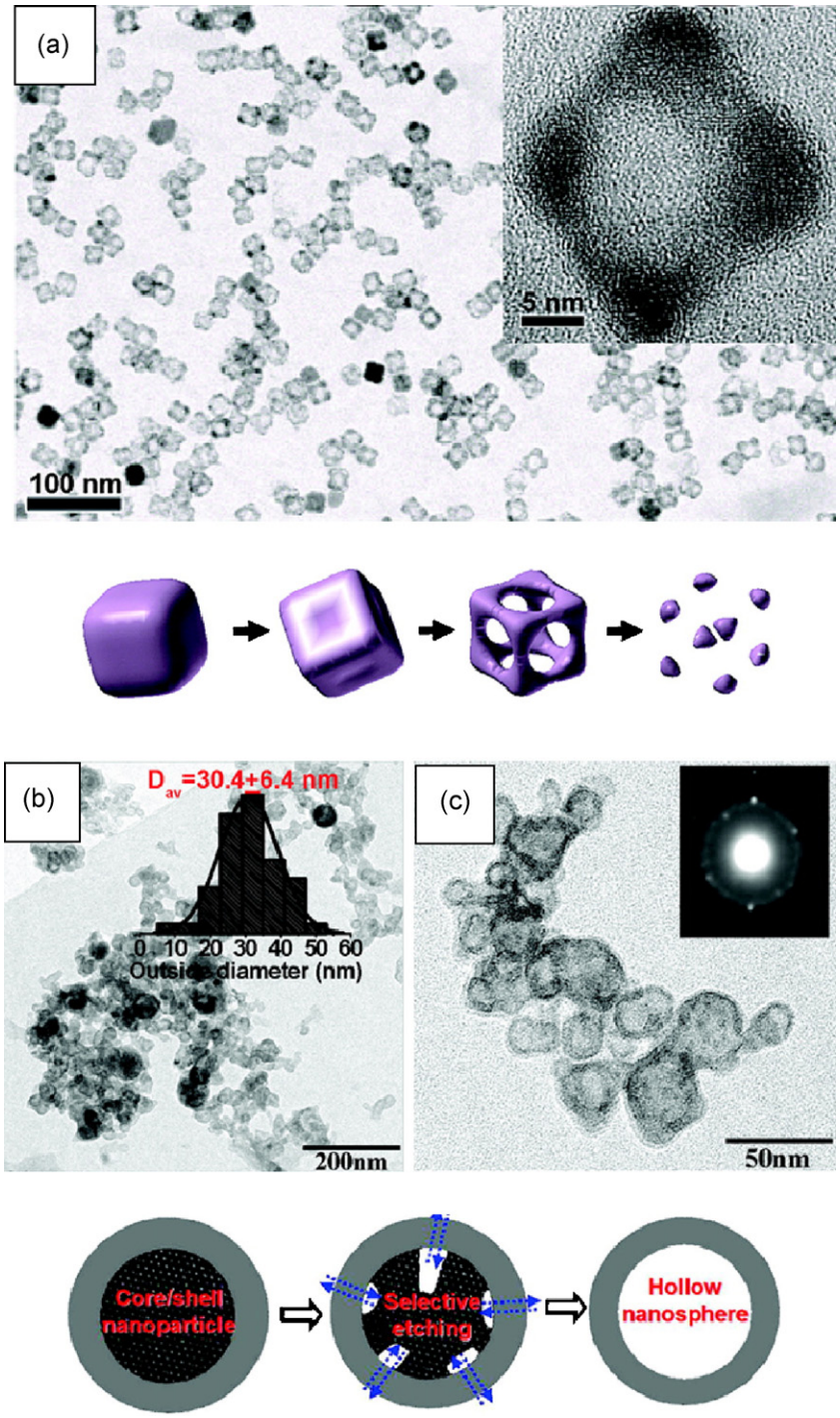

Figure 4 (a) TEM and HRTEM (inset) images of the Fe nanoframes and the overall shape evolution of the Fe nanoparticles in the lower panel (reproduced with permission from [54], copyright 2007 American Chemical Society). (b and c) TEM images of ZnO hollow nanoparticles and the corresponding diameter distribution and electron diffraction pattern in the insets. Schematic illustration of the selective etching strategy for ZnO hollow nanoparticles using a sacrificial template is shown in the lower (reproduced with permission from [57], copyright 2008 American Chemical Society).

sodium molten salt derived from sodium oleate in the solution during the aging process at 380 °C. The molten salt corrosion is a well-known etching process of metal and it was suggested that in situ generated sodium salts in the solution corrode (1 1 0) facets of the preformed iron nanocubes selectively to transform them into nanoframes (Fig. 4a, lower panel). Similarly, Wang et al. synthesized cobalt nanocages and skeletons through NaF-assisted etching of cobalt nanocube aggregates [55]. Xiong et al. reported corrosion-based synthesis of palladium nanoboxes [56]. They reported that the local corrosion of the surface of the nanocubes capped with poly(vinyl pyrrolidone) (PVP) took place at the initial stage of the oxidative etching of palladium nanocubes by O_2 dissolved in the solvent. Further

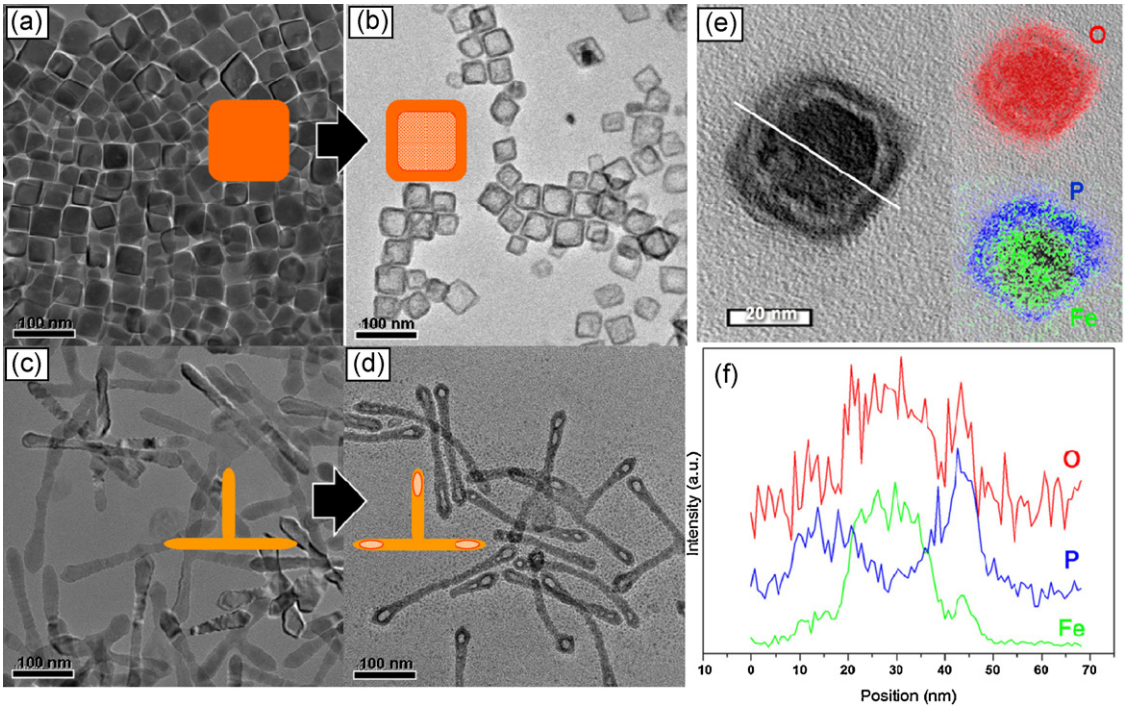

Figure 5 (a–d) TEM images of α-Fe_2O_3 nanocubes (a) and dumbbell-shaped solid MnO nanocrystals (c) and the corresponding hollow oxide nanoparticles obtained via the etching process (b and d). (e) HRTEM image of the core–shell–void intermediate sampled during the etching of α-Fe_2O_3 nanocubes in the left panel. The elemental mapping images for oxygen (red, upper) and iron and phosphorus (green and blue, lower) from electron energy loss spectroscopy (EELS) analysis are shown superimposed on the same TEM image in the right panels. (f) The plots for the relative abundance of each element as functions of position which were measured by energy dispersive X-ray spectroscopy (EDX) on the core–shell–void intermediate (reproduced with permission from [22], copyright 2008 American Chemical Society). (For interpretation of the references to color in this figure legend, the reader is referred to the web version of the article.)

etching dissolved away the core of the nanocubes while the shell was left intact, resulting in the formation of palladium nanoboxes.

Recently, Zeng and co-workers developed a weak acid selective etching strategy to fabricate oxide-based hollow nanoparticles using metal-oxide core–shell nanostructures (Fig. 4b and c) [57]. In their method, Zn/ZnO core/shell nanoparticles were fabricated via laser ablation of a zinc plate in water and then etched with weak acids such as tartaric acid ($C_4H_6O_6$), chloroauric acid ($HAuCl_4$), and chloroplatinic acid (H_2PtCl_6) in aqueous solutions to form ZnO hollow nanoparticles. Interestingly, gold and/or platinum were successfully inserted into the ZnO hollow nanoparticles using $HAuCl_4$ and H_2PtCl_6 as precursors during the etching process, yielding Au–ZnO, Pt–ZnO, and Au–Pt–ZnO hollow core–shell nanoparticles. Kuo and Huang fabricated Cu_2O nanocages and nanoframes by particle aggregation and a selective acid etching process [58]. In this report, $Cu(OH)_2$ was initially formed from the reaction of $CuCl_2$ and NaOH, then reacted with NH_2OH to produce Cu_2O nanoframes and nanocages. By selective etching of the (1 1 0) facets by HCl, Cu_2O nanoparticles were transformed to the nanoframes.

Very recently, the Hyeon group developed a novel nanoscale etching process for the synthesis of various hollow oxide nanoparticles [22]. Simple heating metal-oxide nanocrystals dispersed in technical grade trioctylphosphine oxide (TOPO) at 300 °C for hours resulted in the formation of hollow nanoparticles retaining the size and shape of the original nanocrystals. Specifically, when α-Fe_2O_3 nanocubes (Fig. 5a) and dumbbell-shaped MnO nanoparticles (Fig. 5c) were used as the starting materials for the etching process, hollow nanoboxes and nanodumbbells were produced, while their morphologies were preserved (Fig. 5b and d). The control experiments revealed that impurities such as alkylphosphonic acids in technical grade TOPO were responsible for the etching process. Elemental mapping analysis showed that the shell is phosphorus-rich while the core retains the composition of metal-oxide (Fig. 5e and f). This result revealed that there was both the inward diffusion of phosphorus atoms which might come from phosphonic acid coordinated onto the surface of the nanocrystals, and the outward diffusion of metal atoms during the etching process, which is reminiscent of the Kirkendall effect. However, the phosphonic acid etching process is different from the Kirkendall effect in that the evolution of the hollow nanostructure is not only the result of the difference between the diffusion rate of phosphorus and metal atoms in solid but also the dissolution of metal atoms into the solution resulting in vacancies in the nanoparticles.

Galvanic replacement

Novel metal nanoparticles have attracted a lot of attention for their unique optical properties induced by surface plas-

mon resonance (SPR) and their many potential applications [59–61]. Upon the irradiation of light, conduction electrons confined in noble metal nanoparticles oscillate collectively at a certain resonance frequency, which is determined by the nature of the metal, the dielectric constant of media, and the size and shape of the nanoparticles [26]. Plasmon resonance results in strong light absorption and scattering at and near the resonance frequency and induces strong field enhancement near the surface of the nanoparticles. This effect has been utilized especially for surface enhanced Raman spectroscopy (SERS) and other non-linear optics. The plasmon resonance frequency of noble metal nanoparticles can be tuned in the range of visible to near infrared (near IR) by controlling their dimensions and morphologies. Among the noble metal nanoparticles with SPR effect, the hollow nanostructures have a very high scattering coefficient and its plasmon resonance frequency can be easily controlled by changing the dimension of the hollow core and the thickness of the shell. Due to these features, as well as their strong biocompatibility, various hollow noble metal nanostructures have attracted a lot of attention for their applications such as bioassay, sensing, and drug delivery system [3,4]. For the synthesis of hollow novel metal nanostructures, the galvanic replacement reaction provides a simple and versatile route. The Xia group has developed various hollow nanostructures of Ag, Au, Pt, and Pd with controlled pore volume and wall thickness via the galvanic replacement reaction [62,63]. This reaction takes place when the metal nanoparticles are in contact with other metal ions of higher reduction potential. For example, the standard reduction potential for AgCl/Ag is 0.22 V. Compared to other noble metals, this value is quite low (0.99 V for $AuCl_4^-$/Au, 0.76 V for $PtCl_4^{2-}$/Pt, and 0.59 V for $PdCl_4^{2-}$/Pd) [3]. Then, when silver nanoparticles co-exist with $AuCl_4^-$ ions in the solution, these ions take electrons from Ag atoms and replace them relieving Ag^+ ions. At the same time, the dissolving silver nanoparticles act as the sacrificial template for the formation of gold nanoparticles. The morphologies of the nanoparticles formed via the galvanic replacement of the sacrificial template are usually hollow structures. Depending on the size and shape of the initial Ag nanoparticles, various hollow noble metal nanostructures were generated, including cubic nanoboxes, nanocages, triangular nanorings, prism-shaped nanoboxes, single-walled nanotubes, and multiple-walled nanoshells or nanotubes [3,4,62–68]. Generally, by controlling the size and morphology of the metal template and the degree of replacement of metal atoms in the template, the shell thickness, porosity, and composition of the hollow structure can be tailored.

In the synthetic process for hollow Au nanoboxes or frames, $HAuCl_4$ is added to the suspension of Ag nanocubes in a controlled manner. The silver template-mediated galvanic replacement reaction is described as follows:

$$3Ag(s) + AuCl_4^-(aq) \rightarrow Au(s) + 3Ag^+(aq) + 4Cl^-(aq).$$

When PVP-capped Ag nanocubes with sharp corners shown in Fig. 6a were reacted with a small amount of $HAuCl_4$, small holes were formed on the faces of the nanocubes in the early stage of the galvanic replacement reaction (Fig. 6b). This indicates that the replacement reaction initiated locally on the sites of steps, point defects, or stacking faults with high surface energy. As the reaction proceeds, the small hole serves as an anode where silver atoms are oxidized. The released electrons from silver atoms migrate to the surface of the nanocube and reduce $AuCl_4^-$ ions to Au atoms which adsorb and grow into an Au shell on the nanocubes epitaxially. During the reaction, the holes on the faces of the nanocubes serve as the dissolution site for the silver and finally the silver nanocubes are converted into Au/Ag alloy nanoboxes with empty interiors (Fig. 6c). When there is a sufficient amount of $HAuCl_4$, the surface holes are gradually closed via the mass transport or direct deposition of Au atoms, generating perfect Au nanoboxes with uniform wall thickness. In the presence of even larger

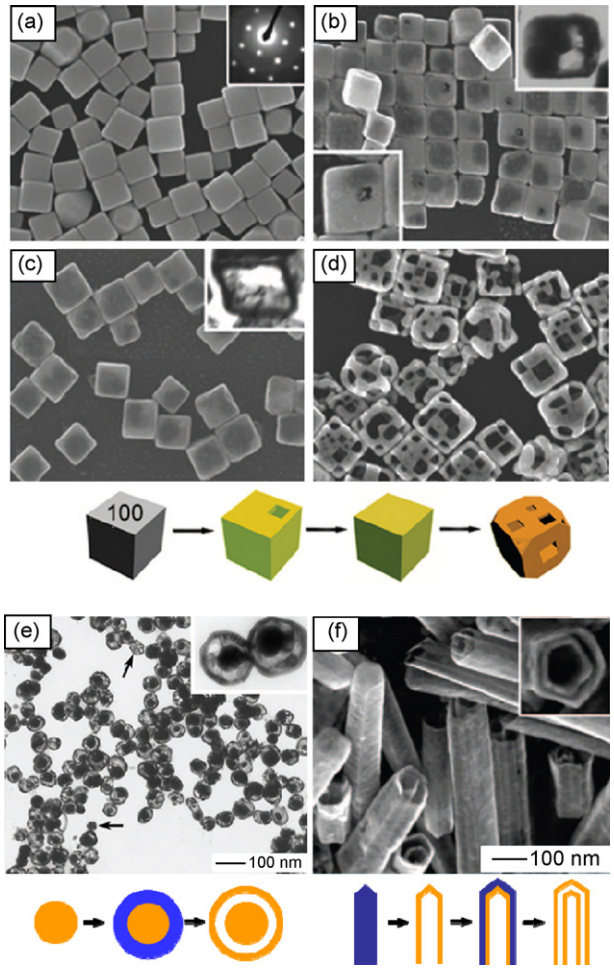

Figure 6 (a–d) SEM images of Ag nanocubes (a), Au/Ag alloy nanocubes with small holes (b), Au/Ag nanoboxes (c), and Au nanocages (d). In the insets, the corresponding TEM and electron diffraction images are shown. The lower panel shows the schematic for the shape evolution during the galvanic replacement reaction (reproduced with permission from [3], copyright 2008 American Chemical Society). (e and f) TEM image of Au/Ag alloy nanorattles (e) and SEM image of multi-walled nanoshells (f). Schematics for the synthetic processes are shown below in which Au/Ag alloy and Ag are colored in orange and blue, respectively (reproduced with permission from [62], copyright 2008 Professional Engineering Publishing).

amounts of $HAuCl_4$, dealloying process takes place and silver atoms in the Au/Ag nanoboxes are selectively removed (Fig. 6d). As the dealloying proceeds further, voids form in the nanoboxes and Au nanoframes with truncated corners are generated, minimizing the total energy of the structure [3,62]. In contrast, when Ag nanocubes with rounded corners are used as the sacrificial template, the replacement reaction occurs at all corners where PVP binds weaker than the other faces, resulting in the formation of Au nanocages with pores on every corner of the cube [3,62]. Furthermore, by coating Au/Ag alloy nanoparticles with silver, interesting hollow structures, such as nanorattles and multi-walled nanoshells or nanotubes can be obtained [3,64—68]. When silver-coated Au/Ag alloy nanoparticles are used as the starting material for galvanic replacement, nanorattles are obtained (Fig. 6e). Similarly, repeating the silver shell coating and galvanic replacement with $AuCl_4^-$ ions leads to the formation of multiple concentric shells [67,68]. Following the same strategy, by using 1-D silver nanoparticles for the replacement reaction, double-walled nanotubes of Au/Ag alloy can be prepared by repeating the replacement reaction (Fig. 6f). Pt/Ag and Pd/Ag hollow structures have also been prepared via the galvanic replacement reaction, because both $PtCl_4^{2-}$ and $PdCl_4^{2-}$ ions have higher standard reduction potential than the AgCl/Ag pair, as mentioned above [69].

Cobalt nanoparticles have also been used as a template for the preparation of noble metal hollow nanostructures via the galvanic replacement reaction [70—76]. Liang et al. have synthesized Pt, Au, and AuPt hollow nanoparticles by using cobalt nanoparticles as the template [70—72]. Interestingly, they synthesized AuPt bimetallic hollow tubular nanomaterials using chain-like templates composed of cobalt nanoparticles assembled by the magnetic dipole interaction [71]. Similarly, Zeng et al. prepared necklace-like Au, Pt, and Pd hollow nanostructures by using cobalt nanoparticles as the template which assembled into 1-D structure by the external magnetic field [76].

Nanotemplate-mediated approach

Monodisperse nanoparticles can be utilized as templates for uniform hollow nanomaterials. The Suslick group synthesized hollow hematite (α-Fe_2O_3) nanocrystals by the sonochemical method using carbon nanoparticles as the template [77]. In this procedure, $Fe(CO)_5$ in the solution was sonicated in the presence of spherical carbon nanoparticles with a diameter of 12 nm, resulting Fe/carbon nanocomposite. Upon exposure to air, the Fe shell on the carbon template was oxidized into α-Fe_2O_3. At the same time, auto-ignition of carbon took place, removing the carbon template and hollow nanostructures of α-Fe_2O_3 were obtained. Nano-sized silica has also successfully used as the inner or outer templates to generate hollow nanostructures. The Hyeon group reported a novel wrap—bake—peel (WBP) process, involving the steps of silica coating, heat treatment, and removal of the silica layer. In this process, the phase, morphology, and structure of the nanomaterials can be transformed [23]. For example, β-FeOOH nanoparticles were wrapped with silica shell and then, the β-FeOOH/silica composites were thermally treated at 300 °C for 5 hr in air. During the thermal treatment, spindle-shaped β-FeOOH nanoparticles were transformed into hollow hematite nanocapsules via the thermal dehydroxylation of β-FeOOH (Fig. 7). The silica-coated nanocapsules were further treated under H_2 flow at 500 °C to transform hematite (α-Fe_2O_3) into magnetite (Fe_3O_4) to change their magnetic property. During this process, the silica shell coated on the surface of β-FeOOH nanoparticles played two critical roles: first, it acted as the template for generation of the hollow structures, and second it prevented the aggregation of the core nanoparticles at high temperatures. The silica shell was removed by dispersing iron oxide/silica composite in an aqueous solution of sodium hydroxide with sonication. It seems that the formation of the nanocapsule in the silica shell via thermal treatment is related to the volume reduction resulting from the dehydroxylation. Similarly, Yang et al. synthesized novel hollow silica nanoparticles via the so-called wrap—melt—bake process [78]. They used magnetically assembled Fe_3O_4 nanoparticles as the template for the large cavity inside the silica nanoparticles. During the synthesis, clusters of Fe_3O_4 nanoparticles bound together with PVP were wrapped with silica shell using the Stöber method [79]. After removing the Fe_3O_4 core with hydrochloric acid and calcinating the shell at high temperatures, hollow silica nanoparticles (with a diameter of ~80 nm and a large pore size of ~45 nm) were obtained.

Organic micelles have been also utilized as the template. The Hyeon group reported uniform goethite (α-FeOOH) nanotubes having a parallelogram cross-section when reacting hydrazine with Fe—oleate complex in reverse micelles [80]. In this reaction, the reverse micelles were formed by mixing oleic acid, xylene, and water and functioned as the soft template for the formation of the nanotubes. In the three approaches for the synthesis of hollow nanostructures that we discussed so far, the role of the surfactants has not been clearly addressed. It has been known that the surfactants bound to the surface of nanoparticles contribute to controlling the shape of the nanoparticles. Although only a few studies on the role of surfactants on hollow nanostructure formation have been published so far, there are some suggestive results. The Park group recently reported the synthesis of parallelepiped cobalt hollow nanoparticles using CoO nanocrystals as the starting material [81]. From the mechanism study, they found that fcc CoO was reduced to fcc cobalt by oleylamine bound to the cobalt cation on the surface of CoO nanocrystals at high temperatures. Also, various hollow or tubular metal-oxide nanostructures were synthesized under hydrothermal/solvothermal conditions using strong binding surfactants onto the specific facets of the nanoparticles [82,83].

Biomedical applications of hollow nanostructures

In these days, considerable progress has been made to deliver biomolecules and drugs to target organs by using various functional nanocarriers that realize simultaneous diagnosis and therapy [84—93]. Hollow silica materials have been used as drug delivery vehicles for their many advantages such as biocompatibility, excellent chemical stability,

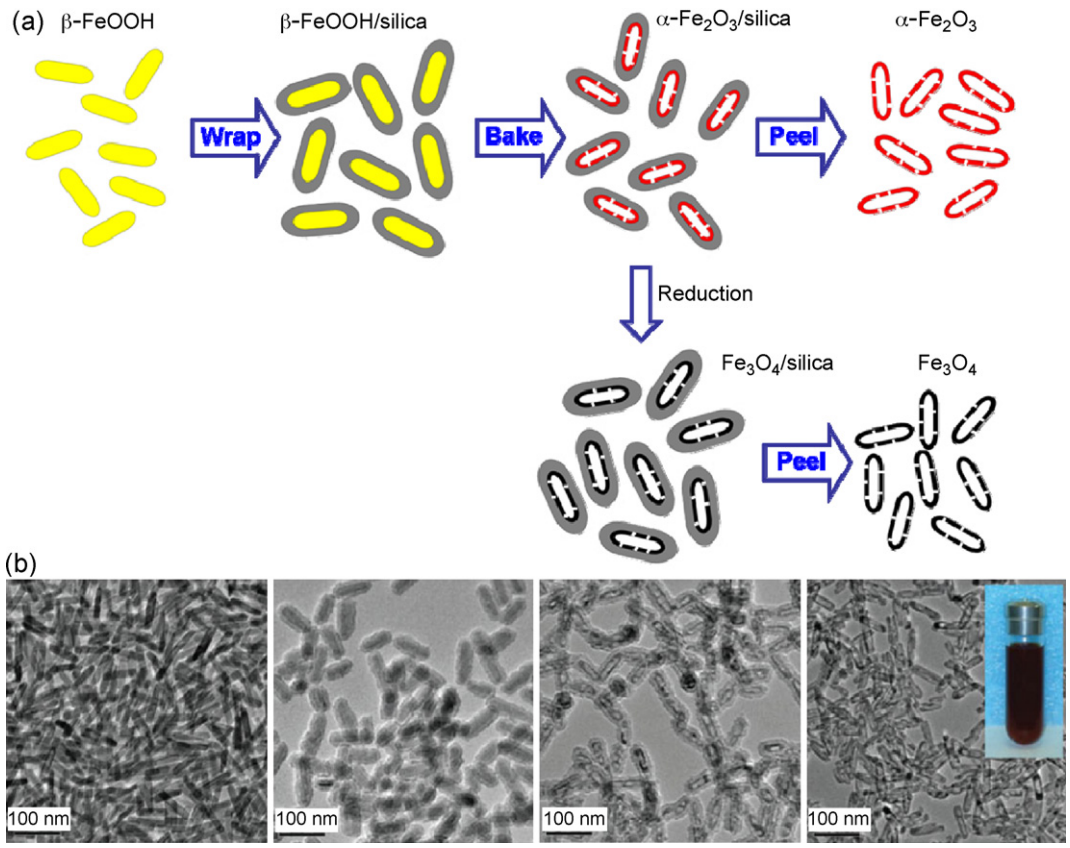

Figure 7 (a) Schematic illustration of the wrap—bake—peel process for the synthesis of uniform-sized iron oxide nanocapsules. (b) TEM images of β-FeOOH nanoparticles, silica-coated β-FeOOH nanoparticles, silica-coated iron oxide nanocapsules after the thermal treatment, and iron oxide nanocapsules after removing silica shell, in order from left to right. The inset is a picture of the water dispersion of iron oxide nanocapsules (reproduced with permission from [23], Copyright 2008 Nature Publishing Group).

and ease of bioconjugation via silane chemistry [29,30,92]. One or more specific nanomaterials can be integrated into the silica nanomaterials to form multifunctional systems. However, the large sizes of silica particles, which often exceed 200 nm, have limited their utility in biological applications. As mentioned previously, Yang et al. synthesized hollow silica nanoparticles with large pores for drug delivery [78]. Doxorubicin (DOX), a potent chemotherapeutic drug, was easily loaded into the pore of the hollow nanoparticles by mixing the hollow nanomaterials with drugs. The drug uptake seems to be proceeded by the concentration gradient between a buffer solution and pores in the nanomaterials. The nanoscale wall thickness and high porosity of the hollow nanomaterials enable drugs and fluorescent molecules to penetrate into the pores. To impart controlled-release ability, the hydroxyl surface of hollow silica nanoparticles were modified with amine to induce a positive surface charge, and then covered with poly(ethylene glycol) (PEG), a process often called ''PEGylation'' [29,30]. Notable sustained drug release was observed from the amine-modified hollow nanoparticles due to the stronger ionic interaction of the DOX carboxylic group with the amine group of the hollow nanoparticles, compared to the hydroxyl-terminated hollow nanoparticles, demonstrating their potential application as a controlled drug delivery vehicle.

Recently, magnetic nanoparticles have attracted much interest for their applications as contrast agents for magnetic resonance imaging (MRI) [94,95]. Since superparamagnetic iron oxide (SPIO) nanoparticles were first used as the contrast agent for the liver, magnetic iron oxide nanoparticles have been used extensively as T_2 MRI contrast agents due to their high magnetic moment compared to other contrast agents such as magnetic metal complexes [29,30,95]. The magnetite hollow nanocapsules developed by the Hyeon group were utilized as multifunctional nanocarriers to deliver drugs and provide contrast for MRI [23]. Fig. 8a shows the T_2 contrast effect of the nanocapsules. When the DOX-loaded nanocapsules were incubated with the breast carcinoma cell line, SKBR3, increased cytotoxicity was observed compared to free DOX, demonstrating the ability of these nanocapsules to act as a drug delivery vehicle (Fig. 8b). Similarly, Wu et al. developed porous iron oxide nanocapsules as drug delivery vehicles [96]. Fluorescent molecules were incorporated into the porous iron oxide nanorods in order to investigate the release behavior and intracellular delivery in Hela cells. The surface of the nanorods was functionalized with layers of polyelectrolytes such as polyacrylic acid (PAA) and polyethylenimine (PEI). The release of the entrapped fluorescein isothiocyanate (FITC) from the nanocapsules exhibited either controlled- or sustained-release trends, depending on the compactness of the polyelectrolyte shells on the surface of the nanocapsules. Hu et al. also reported stimuli-responsive drug release behavior of PVP-modified silica/Fe_3O_4 core/shell

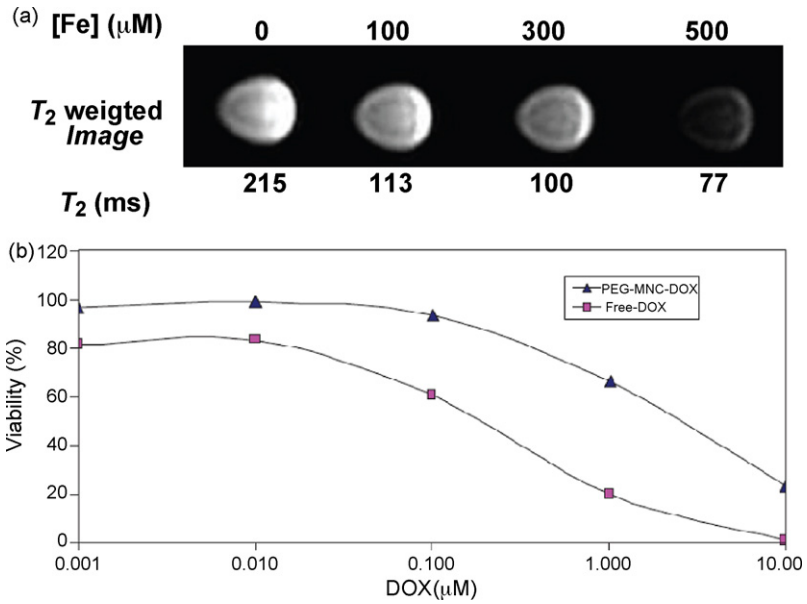

Figure 8 (a) T_2-weighted magnetic resonance images of the magnetite nanocapsules. (b) In vitro cytotoxicity of free DOX and DOX-loaded magnetite nanocapsules against SKBR3 cells (reproduced with permission from [23], Copyright 2008 Nature Publishing Group).

nanoparticles [97]. These core/shell nanoparticles showed surprisingly good controlled release and non-release of fluorescent molecules encapsulated inside of the silica core. The dense, single crystalline Fe_3O_4 shell efficiently prevented the undesired, spontaneous release of the fluorescent dye during the course of delivery. When the nanoparticles reached the disease site, a high-frequency magnetic field was exerted and the molecules encapsulated in the core were released due to rupturing of the shell under the alternating magnetic field.

In addition to being useful as nanocarriers for drug delivery, hollow nanoparticles have been utilized for diagnostics and therapeutics in many ways. The Xu group synthesized FePt—CoS_2 yolk—shell nanoparticles via the nanoscale Kirkendall effect using FePt/Co core/shell nanoparticles as the starting material and evaluated the cytotoxicity of

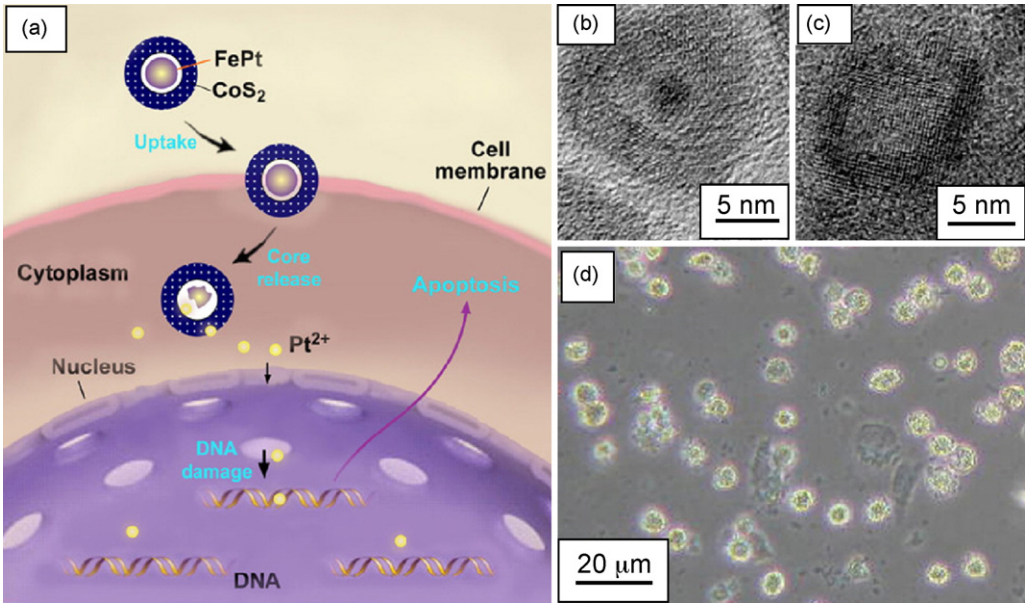

Figure 9 (a) Schematic illustration of the possible mechanism accounts for FePt/CoS_2 yolk/shell nanocrystals killing HeLa cells. (b and c) HRTEM images of FePt/CoS_2 yolk—shell nanoparticles in mitochondria of HeLa cells (b) and hollow CoS_2 nanoparticles after the FePt cores were diffused out to mitochondria (c) (reproduced with permission from [98], copyright 2007 American Chemical Society). (d) The optical image of HeLa cells incubated with 5 μg/mL of FePt/CoS_2 nanoparticles for 3 days (reproduced with permission from [26], copyright 2008 Elsevier).

FePt—CoS_2 yolk—shell nanoparticles [26,98]. After cellular uptake, Pt atoms were released from the FePt core and diffused through the CoS_2 shell. It was shown that these Pt atoms had about 7 times higher cytotoxicity compared to cisplatin in terms of the amount of Pt. According to the data, HeLa cells incubated with 5 μg/mL of FePt—CoS_2 yolk—shell nanoparticles were killed after uptake of the nanoparticles. Fig. 9a shows the plausible mechanism of the cytotoxicity of FePt—CoS_2 yolk—shell nanoparticles against the HeLa cells. After cellular uptake through the endocytic pathway, FePt cores were oxidized and destroyed to yield Fe^{3+} and Pt^{2+} species. The permeability of CoS_2 shells allows these Pt^{2+} species to diffuse out of shells easily. Next, the Pt^{2+} species enter the nucleus and mitochondria, bind to DNA, and lead to apoptosis of the cell. Comparing Fig. 9b and c, it can be seen that the FePt core disintegrated after cellular uptake. They also fabricated bifunctional FePt—Fe_2O_3 yolk—shell nanoparticles that exhibited high cytotoxicity from the FePt yolks and a strong contrast effect for MRI from the γ-Fe_2O_3 shells [99]. Surface functionalized with disease-specific molecules, the yolk—shell nanoparticles could target tumor cells or tissues and detect the transformation of the tumor noninvasively using MRI.

The Xia group developed hollow Au nanocages as cancer-targeting nanoprobes for bioimaging and photothermal therapy agents. Au nanoparticles are especially advantageous for biomedical applications because of their compact size, biocompatibility, chemical stability, and excellent bioconjugation ability via Au-thiolate chemistry [3,4]. The Au nanocages with a dimension of ~40 nm have SPR peaks around 800 nm, a common range used for optical coherence tomography (OCT) imaging [4,100]. Since the image contrast in OCT mainly comes from the scattering and absorption of light by tissues, both the sensitivity and specificity of OCT depend strongly on the intrinsic optical properties of the biological sample. In OCT measurements, Au nanocages strongly absorbed light in the near-IR region with an absorption cross-section 5 orders of magnitude higher than the most commonly used contrast agent such as indocyanine green (ICG). This result suggests their potential use as

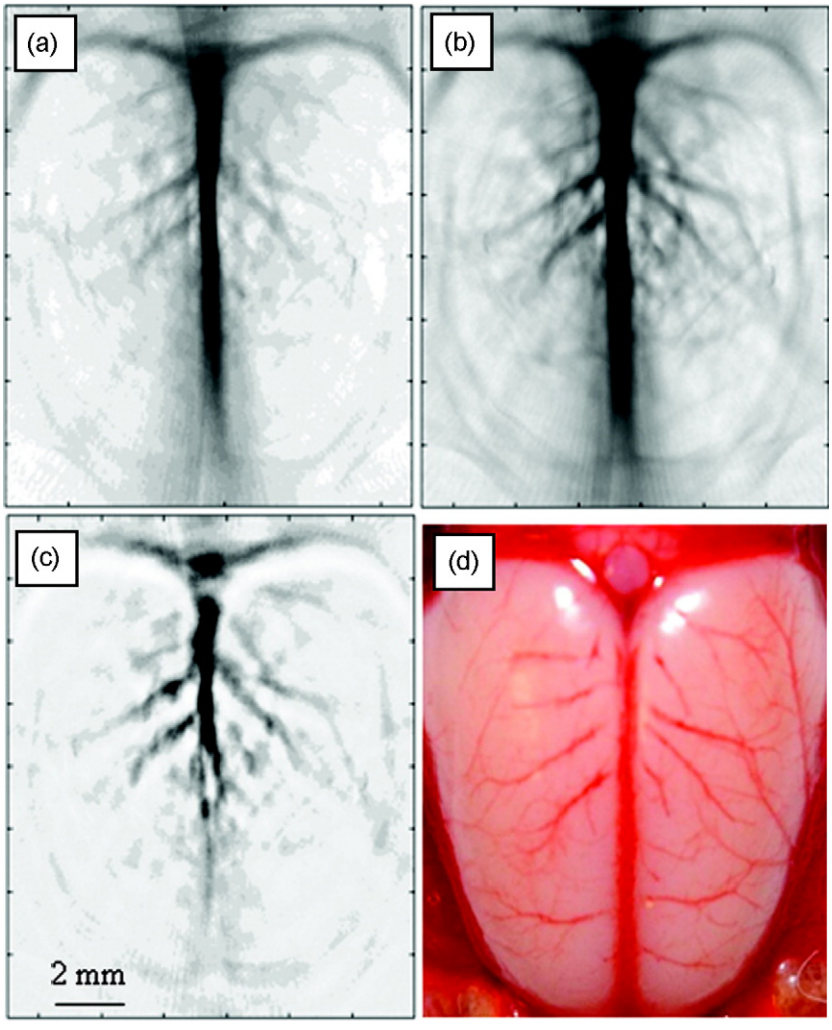

Figure 10 (a and b) PAT images of a rat's cerebral cortex before (a) and about 2 h after the final injection of PEGylated Au nanocages (b), which is the peak enhancement point. (c) A differential PAT image. (d) An open-skull photograph of the rat's cerebral cortex, revealing features of the vasculature (reproduced with permission from [101], copyright 2007 American Chemical Society).

an efficient contrast agent for optical diagnostics of cancers. Also, the *in vivo* use of Au nanocages as contrast enhancement agents for photoacoustic tomography (PAT) was demonstrated [3,101,102]. PAT combines the merits of both optical and ultrasonic imaging by measuring the ultrasonic waves originated from the thermoelastic expansion of tissue upon the absorption of light. It provides higher spatial resolution than purely optical imaging in deep tissues and can overcome the disadvantages of ultrasonic imaging, such as low biochemical contrast and the speckle artifact [101]. It was shown that Au nanocages can be used in PAT to enhance the contrast between blood and the surrounding tissues. As shown in Fig. 10a and b, after three successive injections of PEGylated Au nanocages, a gradual enhancement of the optical absorption in the cerebral cortex of a rat, by up to 81%, was observed. A differential optical absorption image (Fig. 10c) and a photograph of the open skull (Fig. 10d) reveal that the anatomical features of the vasculature match well with those of PAT images, which shows the effectiveness of Au nanocages for the contrast enhancement in PAT. Compared with Au nanoshells, Au nanocages appear to be more effective for PAT due to their larger absorption cross-section. The large absorption cross-section of Au nanocages leads to a strong photothermal effect, by which absorbed photons are converted into heat. It has been demonstrated that *in vitro* photothermal destruction of breast cancer cells is possible with antibody-functionalized Au nanocages [100,103–105].

Conclusions and outlook

In the past few years, there have been considerable advancements concerning the synthesis of hollow materials. Several synthetic strategies capable of synthesizing uniform hollow nanomaterials have been developed so far. We categorize these strategies into four main classes: (1) Kirkendall effect, (2) chemical etching, (3) galvanic replacement, and (4) template-mediated approaches. Each approach has its own advantages. The Kirkendall effect, based on mass transport through the interface between different solid phases, is the most general and well-understood process. This approach has been applied for synthesizing hollow nanostructures of various metal-oxides, chalcogenides, and some phosphides. There is a diversity of chemical etching reaction routes used to form hollow nanostructures, including molten salt corrosion, oxidative etching, and acid etching. The galvanic replacement is a simple method, especially for the synthesis of noble metal hollow nanoparticles. Using silver nanoparticles as the sacrificial template, hollow nanostructures of various morphologies have been fabricated. Template-mediated approaches are effective and easily controllable methods and have been applied for the synthesis of hollow silica and iron oxide nanoparticles.

The large pore volume as well as the small size and their other useful properties such as magnetism and plasmon resonance make hollow nanoparticles promising candidates for use as multimodal nanoprobe/carriers for both drug delivery and bioimaging. Until now, there have been several reports on the utility of hollow nanoparticles for diagnostics and therapeutics. Hollow silica and metal-oxide nanoparticles have been utilized as drug delivery systems exhibiting extended drug release. Hollow nanoparticles composed of magnetic metal-oxide have the contrast enhancement effect necessary for MRI. Furthermore, it was demonstrated that magnetic hollow nanoparticles can be used for drug release by magnetic stimulation. Other than drug delivery, yolk–shell nanoparticles with a cytotoxic core were used for therapeutics inducing apoptosis of cancer cells. Noble metal hollow nanoparticles have interesting optical properties due to the SPR effect. Using Au nanocages with high scattering and absorption coefficients, contrast enhancement in optical imaging and the photothermal effect for therapeutics were achieved.

We anticipate that, by manipulating the physical, chemical, and biological properties of hollow nanomaterials, it will be possible to design and fabricate hollow nanomaterials to utilize them for the biomedical applications enabling to carry out diagnosis and therapy simultaneously. For this purpose, we need further studies on many issues including the biocompatibility, *in vivo* targeting efficiency, and long-term stability of hollow nanomaterials.

Acknowledgements

We acknowledge financial support by the Korean Ministry of Education, Science and Technology through the National Creative Research Initiative Program and the World Class University (WCU) program of the Korea Science and Engineering Foundation (KOSEF).

References

[1] X.W. Lou, L.A. Archer, Z. Yang, Adv. Mater. 20 (2008) 3987.
[2] H.J. Fan, U. Gösele, M. Zacharias, Small 3 (2007) 1660.
[3] S.E. Skarabalak, J. Chen, Y. Sun, X. Lu, L. Au, C.M. Cobley, et al., Acc. Chem. Res. 41 (2008) 1587.
[4] J. Chen, F. Saeki, B.J. Wiley, H. Cang, M.J. Cobb, Z.Y-. Li, et al., Nano Lett. 5 (2005) 473.
[5] F. Caruso, R.A. Caruso, H. Mohwald, Science 282 (1998) 1111.
[6] R.A. Caruso, A. Susha, F. Caruso, Chem. Mater. 13 (2001) 400.
[7] F. Caruso, M. Spasova, A. Susha, M. Giersig, R.A. Caruso, Chem. Mater. 13 (2001) 109.
[8] A. Imhof, Langmuir 17 (2001) 3579.
[9] C. Graf, D.L.J. Vossen, A. Imhof, A. van Blaaderen, Langmuir 19 (2003) 6693.
[10] S.W. Kim, M. Kim, W.Y. Lee, T. Hyeon, J. Am. Chem. Soc. 124 (2002) 7642.
[11] X.M. Sun, Y.D. Li, Angew. Chem. Int. Ed. 43 (2004) 3827.
[12] M. Yang, J. Ma, C.L. Zhang, Z.Z. Yang, Y.F. Lu, Angew. Chem. Int. Ed. 44 (2005) 6727.
[13] S.B. Yoon, K. Sohn, J.Y. Kim, C.H. Shin, J.S. Yu, T. Hyeon, Adv. Mater. 14 (2002) 19.
[14] J. Hwang, B.D. Min, J.S. Lee, K. Keem, K. Cho, M.Y. Sung, M.S. Lee, S. Kim, Adv. Mater. 16 (2004) 422.
[15] D.H.M. Buchold, C. Feldmann, Nano Lett. 7 (2007) 3489.
[16] Y.S. Li, J.L. Shi, Z.L. Hua, H.R. Chen, M.L. Ruan, D.S. Yan, Nano Lett. 3 (2003) 609.
[17] Q. Peng, Y.J. Dong, Y.D. Li, Angew. Chem. Int. Ed. 42 (2003) 3027.
[18] C.Z. Wu, Y. Xie, L.Y. Lei, S.Q. Hu, C.Z. OuYang, Adv. Mater. 18 (2006) 1727.
[19] S.S. Kim, W.Z. Zhang, T.J. Pinnavaia, Science 282 (1998) 1302.
[20] H.L. Xu, W.Z. Wang, Angew. Chem. Int. Ed. 46 (2007) 1489.
[21] Y. Yin, R. Rioux, C.K. Erdonmez, S. Hughes, G.A. Somorjai, A.P. Alivisatos, Science 304 (2004) 711.

[22] K. An, S.G. Kwon, M. Park, H.B. Na, S.-I. Baik, J.H. Yu, et al., Nano Lett. 8 (2008) 4252.
[23] Y. Piao, J. Kim, H.B. Na, D. Kim, J.S. Baek, M.K. Ko, et al., Nat. Mater. 7 (2008) 242.
[24] M. De, P.S. Ghosh, V.M. Rotello, Adv. Mater. 20 (2008) 4225.
[25] M. Vallet-Regí, F. Balas, D. Arcos, Angew. Chem. Int. Ed. 46 (2007) 7548.
[26] J. Gao, B. Xu, Nano Today 4 (2009) 37.
[27] V.S. Maceia, M.A.C. Correa-Duarte, Adv. Mater. 19 (2007) 4131.
[28] H. Zeng, S. Sun, Adv. Funct. Mater. 18 (2008) 391.
[29] Y. Piao, A. Burns, J. Kim, U. Wiesner, T. Hyeon, Adv. Funct. Mater. 18 (2008) 3745.
[30] J. Kim, Y. Piao, T. Hyeon, Chem. Soc. Rev. 38 (2009) 372.
[31] E.O. Kirkendall, Trans. AIME 147 (1942) 104.
[32] A.D. Smigelskas, E.O. Kirkendall, Trans. AIME 171 (1947) 130.
[33] Y. Yin, C.K. Erdonmez, A. Cabot, S. Hughes, A.P. Alivisatos, Adv. Funct. Mater. 16 (2006) 1389.
[34] S. Peng, S. Sun, Angew. Chem. Int. Ed. 46 (2007) 4155.
[35] A. Cabot, V.F. Puntes, E. Shevchenko, Y. Yin, L. Balcells, M.A. Marcus, et al., J. Am. Chem. Soc. 129 (2007) 10358.
[36] H.J. Fan, M. Knez, R. Scholz, K. Nielsch, E. Pippel, D. Hesse, et al., Nat. Mater. 5 (2006) 627.
[37] H.J. Fan, M. Knez, R. Scholz, D. Hesse, K. Nielsch, M. Zacharias, et al., Nano Lett. 7 (2007) 993.
[38] J. Gao, B. Zhang, X. Zhang, B. Xu, Angew. Chem. Int. Ed. 45 (2006) 1220.
[39] A.E. Henkes, Y. Vasquez, R.E. Schaak, J. Am. Chem. Soc. 129 (2007) 1896.
[40] R.-K. Chiang, R.-T. Chiang, Inorg. Chem. 46 (2007) 369.
[41] W. Liang, X. Wang, Y. Zhuang, B. Xu, S. Kuang, Y. Li, J. Am. Chem. Soc. 130 (2008) 2736.
[42] E.V. Shevchenko, M.I. Bodnarchuk, M.V. Kovalenko, D.V. Talapin, R.K. Smith, S. Aloni, et al., Adv. Mater. 20 (2008) 4323.
[43] A. Cabot, R.K. Smith, Y. Yin, H. Zheng, B.M. Reinhard, H. Liu, et al., ACS Nano 2 (2008) 1452.
[44] E.V. Shevchenko, J.B. Kortright, D.V. Talapin, S. Aloni, A.P. Alivisatos, Adv. Mater. 19 (2007) 4183.
[45] S. Zhou, B. Varughese, B. Eichhorn, G. Jackson, K. McIlwrath, Angew. Chem. Int. Ed. 44 (2005) 4539.
[46] H. Cao, X. Qian, J. Zai, J. Yin, Z. Zhu, Chem. Commun. (2006) 4548.
[47] Y. Chang, M.L. Lye, H.C. Zeng, Langmuir 21 (2005) 3746.
[48] C. Hwee, B. Ng, H. Tan, W.Y. Fan, Langmuir 22 (2006) 9717.
[49] H. Tan, S. Li, W.Y. Fan, J. Phys. Chem. B 110 (2006) 15812.
[50] Y. Wang, L. Cai, Y. Xia, Adv. Mater. 17 (2005) 473.
[51] X. Chen, Z. Zhang, Z. Qiu, C. Shi, X. Li, J. Colloid Interface Sci. 308 (2007) 271.
[52] H.F. Shao, X.F. Qian, Z.K. Zhu, J. Solid State Chem. 178 (2005) 3522.
[53] R. Nakamura, J.-G. Lee, D. Tokozakura, H. Mori, H. Nakajima, Mater. Lett. 61 (2007) 1060.
[54] D. Kim, J. Park, K. An, N.-K. Yang, J.-G. Park, T. Hyeon, J. Am. Chem. Soc. 129 (2007) 5812.
[55] X. Wang, H. Fu, A. Peng, T. Zhai, Y. Ma, F. Yuan, et al., Adv. Mater. 21 (2009) 1636.
[56] Y. Xiong, B. Wiley, J. Chen, Z.-Y. Li, Y. Yin, Y. Xia, Angew. Chem. Int. Ed. 44 (2005) 7913.
[57] H. Zeng, W. Cai, P. Liu, X. Xu, H. Zhou, C. Klingshirn, H. Kalt, ACS Nano 2 (2008) 1661.
[58] C.-H. Kuo, M.H. Huang, J. Am. Chem. Soc. 130 (2008) 12815.
[59] U. Kreibig, M. Vollmer, Optical Properties of Metal Clusters, Springer, Berlin, 1995.
[60] S. Eustis, M.A. El-Sayed, Chem. Soc. Rev. 35 (2006) 209.
[61] W.A. Murray, W.L. Barnes, Adv. Mater. 19 (2007) 3771.
[62] X. Lu, J. Chen, S.E. Skrabalak, Y. Xia, Proc. ImechE. 221 (2008) 1.
[63] S.E. Skrabalak, L. Au, X. Li, Y. Xia, Nat. Protoc. 2 (2007) 2182.
[64] Y. Sun, Y. Xia, Adv. Mater. 15 (2003) 695.
[65] Y. Khalavka, J. Becker, C. Sönnichsen, J. Am. Chem. Soc. 131 (2009) 1871.
[66] Y. Sun, Y. Xia, J. Am. Chem. Soc. 126 (2004) 3892.
[67] Y. Sun, B.J. Wiley, Z.-Y. Li, Y. Xia, J. Am. Chem. Soc. 126 (2004) 9399.
[68] Y. Sun, Y. Xia, Adv. Mater. 16 (2004) 264.
[69] J. Chen, B. Wiley, J. McLellan, Y. Xiong, Z.-Y. Li, Y. Xia, Nano Lett. 5 (2005) 2058.
[70] H.-P. Liang, L.-J. Wan, C.-L. Bai, L. Jiang, J. Phys. Chem. B 109 (2005) 7795.
[71] H.-P. Liang, Y.G. Guo, H.M. Zhang, J.S. Hu, L.J. Wan, C.L. Bai, Chem. Commun. (2004) 1496.
[72] H.-P. Liang, H.-M. Zhang, J.-S. Hu, Y.-G. Guo, L.-J. Wan, C.-L. Bai, Angew. Chem. Int. Ed. 43 (2004) 1540.
[73] M. Chen, L. Gao, Inorg. Chem. 45 (2006) 5145.
[74] S. Guo, Y. Fang, S. Dong, E. Wang, J. Phys. Chem. C 111 (2007) 17104.
[75] Y. Vasquez, A.K. Sra, R.E. Schaak, J. Am. Chem. Soc. 127 (2005) 12504.
[76] J. Zeng, J. Huang, W. Lu, X. Wang, B. Wang, S. Zhang, et al., Adv. Mater. 19 (2007) 2172.
[77] J.H. Bang, K.S. Suslick, J. Am. Chem. Soc. 129 (2007) 2242.
[78] J. Yang, J. Lee, J. Kang, K. Lee, J.-S. Suh, H.-G. Yoon, et al., Langmuir 24 (2008) 3417.
[79] W. Stöber, A. Fink, E. Bohn, J. Colloid Interface Sci. 26 (1968) 62.
[80] T. Yu, J. Park, J. Moon, K. An, Y. Piao, T. Hyeon, J. Am. Chem. Soc. 129 (2007) 14558.
[81] K.M. Nam, J.H. Shim, H. Ki, S.-I. Choi, G. Lee, J.K. Jang, et al., Angew. Chem. Int. Ed. 47 (2008) 9504.
[82] C.-J. Jia, L.-D. Sun, Z.-G. Yan, L.-P. You, F. Luo, X.-D. Han, et al., Angew. Chem. Int. Ed. 44 (2005) 4328.
[83] X. Hu, J.C. Yu, J. Gong, Q. Li, G. Li, Adv. Mater. 19 (2007) 2324.
[84] V. Sokolova, M. Epple, Angew. Chem. Int. Ed. 47 (2008) 1382.
[85] J. Dohson, Drug Dev. Res. 67 (2006) 55.
[86] M. Liong, J. Lu, M. Kovochich, T. Xia, S.G. Ruehm, A.E. Nel, et al., ACS Nano 2 (2008) 889.
[87] A. Yan, B.W. Lau, B.S. Weissman, I. Külaots, N.Y.C. Yang, A.B. Kane, et al., Adv. Mater. 18 (2006) 2373.
[88] S. Moudgil, J.Y. Ying, Adv. Mater. 19 (2007) 3130.
[89] J. Liu, A. Stace-Naughton, X. Jiang, C.J. Brinker, J. Am. Chem. Soc. 131 (2009) 1345.
[90] W.J. Rieter, K.M. Pott, K.M.L. Taylor, W. Lin, J. Am. Chem. Soc. 130 (2008) 11584.
[91] H. Park, J. Yang, S. Seo, K. Kim, J. Suh, D. Kim, et al., Small 4 (2008) 192.
[92] J. Lu, M. Liong, J.I. Zink, F. Tamanoi, Small 3 (2007) 1341.
[93] G.B. Sukhorukov, A.L. Rogach, B. Zebli, T. Liedl, A.G. Skirtach, K. Köhler, Small 1 (2005) 194.
[94] H.B. Na, J.H. Lee, K. An, Y.I. Park, M. Park, I.S. Lee, et al., Angew. Chem. Int. Ed. 46 (2007) 5397.
[95] H.B. Na, I.C. Song, T. Hyeon, Adv. Mater. 21 (2009) 2133.
[96] P.-C. Wu, W.-S. Wang, Y.-T. Huang, H.-S. Sheu, Y.-W. Lo, T.-L. Tsai, et al., Chem. Eur. J. 13 (2007) 3878.
[97] S.-H. Hu, S.-Y. Chen, D.-M. Liu, C.-S. Hsiao, Adv. Mater. 20 (2008) 2690.
[98] J. Gao, G. Liang, B. Zhang, Y. Kuang, X. Zhang, B. Xu, J. Am. Chem. Soc. 129 (2007) 1428.
[99] J. Gao, G. Liang, J.S. Cheung, Y. Pan, Y. Kuang, F. Zhao, et al., J. Am. Chem. Soc. 130 (2008) 11828.
[100] J. Chen, B. Wiley, Z.-Y. Li, D. Campbell, F. Saeki, H. Chang, et al., Adv. Mater. 17 (2005) 2255.
[101] X. Yang, S.E. Skrabalak, Z.-Y. Li, Y. Xia, L.V. Wang, Nano Lett. 7 (2007) 3798.

[102] Y. Wang, X. Xie, X. Wang, G. Ku, K.L. Gill, D.P. O'Neal, et al., Nano Lett. 4 (2004) 1689.
[103] J. Chen, D. Wang, J. Xi, L. Au, A. Siekkinen, A. Warsen, et al., Nano Lett. 7 (2007) 1318.
[104] L. Au, D. Zheng, F. Zhou, Z.-Y. Li, X. Li, Y. Xia, ACS Nano 2 (2008) 1645.
[105] M. Hu, J. Chen, Z.-Y. Li, L. Au, G.V. Hartland, X. Li, et al., Chem. Soc. Rev. 35 (2006) 1084.

Kwangjin An received his BS (2003) in the School of Chemical Engineering from Chungnam National University and his PhD (2009) in the School of Chemical and Biological Engineering from Seoul National University. During his PhD course under the direction of professor Taeghwan Hyeon, he had conducted research on the synthesis and characterization of monodisperse metal-oxide nanocrystals. He is currently a postdoctoral researcher working with professor Taeghwan Hyeon at Seoul National University.

Taeghwan Hyeon received his BS (1987) and MS (1989) in chemistry from the Seoul National University. He obtained his PhD in chemistry from the University of Illinois at Urbana-Champaign (1996). Since he joined the faculty of the School of Chemical and Biological Engineering of Seoul National University in September 1997, he has been focused on the synthesis and applications of uniform-sized nanocrystals and nanoporous materials, and he published more than 120 papers in prominent international journals. He is currently a Director of National Creative Research Initiative Center for Oxide Nanocrystalline Materials supported by the Korean Ministry of Education, Science and Technology. He received many awards including the Korean Young Scientist Award from the Korean President (2002), DuPont Science and Technology Award (2005), and POSCO-T. J. Park Award (2008). He is currently serving as editorial board member of *Advanced Materials*, *Chemical Communications*, *Chemistry of Materials*, *International Journal of Nanotechnology*, and *Small*.